



ARTICLE

Dihydro-stilbene gigantol relieves CCl₄-induced hepatic oxidative stress and inflammation in mice via inhibiting C5b-9 formation in the liver

Ya-ru Xue^{1,2}, Sheng Yao^{1,3,4}, Qian Liu^{1,2}, Zhao-liang Peng¹, Qiang-qiang Deng¹, Bo Liu^{1,2}, Zheng-hua Ma^{3,4,5}, Le Wang^{1,2}, Hu Zhou^{1,2}, Yang Ye^{1,3,4,5} and Guo-yu Pan^{1,2}

In general, anti-inflammatory treatment is considered for multiple liver diseases despite the etiology. But current drugs for alleviating liver inflammation have defects, making it necessary to develop more potent and safer drugs for liver injury. In this study, we screened a series of (dihydro-)stilbene or (dihydro-)phenanthrene derivatives extracted from *Pholidota chinensis* for their potential biological activities. Among 31 compounds, the dihydro-stilbene gigantol exerted most potent protective effects on human hepatocytes against lithocholic acid toxicity, and exhibited solid antioxidative and anti-inflammatory effect in vitro. In mice with CCl₄-induced acute liver injury, pre-administration of gigantol (10, 20, 40 mg·kg⁻¹·d⁻¹, *po*, for 7 days) dose-dependently decreased serum transaminase levels and improved pathological changes in liver tissues. The elevated lipid peroxidation and inflammatory responses in the livers were also significantly alleviated by gigantol. The pharmacokinetic studies showed that gigantol was highly concentrated in the mouse livers, which consisted with its efficacy in preventing liver injury. Using a label-free quantitative proteomic analysis we revealed that gigantol mainly regulated the immune system process in liver tissues of CCl₄-treated mice, and the complement and coagulation cascades was the predominant pathway; gigantol markedly inhibited the expression of complement component C9, which was a key component for the formation of terminal complement complex (TCC) C5b-9. These results were validated by immunohistochemistry (IHC) or real time-PCR. Confocal microscopy analysis showed that gigantol significantly inhibited the vascular deposition of TCC in the liver. In conclusion, we demonstrate for the first time that oral administration of gigantol potentially relieves liver oxidative stress and inflammation, possibly via a novel mechanism of inhibiting the C5b-9 formation in the liver.

Keywords: gigantol; Chinese traditional medicine; liver injury; oxidative stress; inflammation; label-free proteomic; complement and coagulation cascades; terminal complement complex

Acta Pharmacologica Sinica (2020) 41:1433–1445; <https://doi.org/10.1038/s41401-020-0406-6>

INTRODUCTION

The liver is the principal organ responsible for substance metabolism and detoxification, which makes it easily attacked by numerous pathogenic factors [1]. When exposed continuously to these factors, the liver is subject to inflammatory injury. Inflammation occurs in all types of chronic and acute liver injury, including alcoholic liver diseases (ALDs), ischemia-reperfusion (I/R)-induced liver injury, and non-alcoholic steatohepatitis (NASH). These inflammatory injuries may progress into fibrosis, cirrhosis, and ultimately hepatocellular carcinoma [2, 3]. Currently, the number of deaths caused by liver diseases globally reaches up to 2 million each year [4].

Reactive oxygen species (ROS) initiates liver inflammation as well as subsequent lipid peroxidation [5], apoptosis [6], and oncotic necrosis [7]. Activated Kupffer cells and neutrophils further

generate ROS and pro-inflammatory mediators, leading to fulminant inflammation [8]. Oxidative stress-induced lipid peroxidation also promotes the transition of hepatic steatosis to NASH, which is characterized by inflammation with or without fibrosis [9]. In general, anti-inflammatory treatment is used for multiple liver diseases regardless of the etiology. However, current drugs used to alleviate liver inflammation have certain shortcomings. For instance, bicyclol may aggravate liver injury in the clinic after drug withdrawal. N-acetylcysteine takes effect only in the very early phase of liver injury [10, 11], and it may lead to electrolyte disturbances when the clinical dose is increased [12]. The poor bioavailability of silymarin (0.73%–0.95%) leads to significant variability issues [13–15]. In addition, few suitable therapeutics have been used for liver diseases such as NASH, which is closely associated with liver inflammation and oxidative stress [16].

¹Shanghai Institute of Materia Medica, Chinese Academy of Sciences, Shanghai 201203, China; ²University of Chinese Academy of Sciences, Beijing 100049, China; ³State Key Laboratory of Drug Research and Natural Products Chemistry Department Shanghai Institute of Materia Medica, Chinese Academy of Sciences, Shanghai 201203, China; ⁴SIMM-CUHK Joint Research Laboratory for Promoting Globalization of Traditional Chinese Medicines, Shanghai 201203, China and ⁵School of Life Science and Technology, Shanghai Tech University, Shanghai 201203, China

Correspondence: Yang Ye (yye@simm.ac.cn) or Guo-yu Pan (gypan@simm.ac.cn)

These authors contributed equally: Ya-ru Xue, Sheng Yao

Received: 5 January 2020 Accepted: 23 March 2020

Published online: 13 May 2020

Therefore, it is necessary for us to develop more potent and safer drugs for liver injury.

Natural products have long been used to treat liver diseases [17]. (Dihydro-)stilbene or (dihydro-)phenanthrene derivatives are universally found in members of the *Orchidaceae* family. They have been reported to potently inhibit nitric oxide (NO) formation and scavenge DPPH radicals [18, 19]. These in vitro anti-inflammatory and antioxidative effects suggest that these natural products may protect the liver from inflammation-induced injury. However, no systematic studies on their therapeutic potential in liver injury have been performed.

In our previous studies, more than thirty (dihydro-)stilbene or (dihydro-)phenanthrene derivatives were isolated from the whole *Pholidota chinensis* plant (the molecular structures of these compounds are listed in Supplementary Fig. S1) [20, 21]. Here, their hepatoprotective, antioxidative, and anti-inflammatory activities were assessed and compared in vitro. Since gigantol showed excellent in vitro activity, in vivo studies were conducted to confirm its exposure and efficacy in mice. Furthermore, label-free quantitative proteomics analysis along with various biochemical methods was used to explore the potential therapeutic mechanisms of gigantol. The bioinformatics analysis revealed that gigantol predominantly regulates the complement and coagulation cascades, in which the expression of complement component C9 was most significantly downregulated. C9 is an important component of the terminal complement complex (TCC) C5b-9, which has been suggested as a pro-inflammatory trigger [22]. The inhibition of C5b-9 formation by gigantol in liver tissues was further validated by various biochemical methods. Overall, these results indicate that gigantol may exert its hepatoprotective effect via a novel mechanism associated with C5b-9 complex, which may be a new therapeutic strategy for relieving liver inflammation.

MATERIALS AND METHODS

Chemicals and biochemical reagents

CCl₄, olive oil, and Tween 80 were purchased from Sinopharm Group Co., Ltd. (Shanghai, China). Lithocholic acid (LCA), silymarin, vitamin C (Vc), dexamethasone (Dex), and lipopolysaccharide (LPS) were obtained from Sigma-Aldrich (St. Louis, MO, USA). 1,1-diphenyl-2-picrylhydrazyl radical 2,2-diphenyl-1-(2,4,6-trinitrophenyl)hydrazyl (DPPH) was purchased from Macklin (Shanghai, China). Acetonitrile and formic acid (high-performance liquid chromatography grade) were purchased from Merck (Darmstadt, Germany). (Dihydro-)stilbene or (dihydro-)phenanthrene derivatives were extracted from *P. chinensis* according to previous reports [20, 21]. Gigantol used for the animal experiment was synthesized according to a previous report [23].

All reagents for cell culture were purchased from Gibco Life Technologies (Carlsbad, CA, USA) unless otherwise stated.

Cell culture and treatment

Cell lines

Human induced hepatocytes (hiHeps): HiHeps were kindly supplied by Professor Li-jian Hui (Shanghai Institutes for Biological Sciences, SIBS). According to previous protocols [24], the cells were cultured on collagen-coated dishes and maintained in hepatocyte maintenance medium. When the confluence reached 90%, the cells were seeded in 96-well plates at a density of 100,000 cells/mL for another 3 days of culture. On the third day, the hiHeps were incubated with LCA (30 μM) or the indicated compounds at different doses. After 24 h of incubation, the cell viability and ROS levels of hiHeps were measured.

L929 cell line: L929 cells were obtained from ATCC and used for the acquisition of macrophage colony stimulating factor (M-CSF). The cells were maintained in high-glucose DMEM containing 10% FBS without antibiotics. To obtain M-CSF, L929 cells were cultured

in dishes for 7 days without replacing the medium. On the 7th day, the cell supernatants were collected and filtered with a filter membrane (0.22 μm; Merck Millipore, Darmstadt, Germany) and stored at -20 °C for subsequent use.

Isolation of primary cells

Rat primary hepatocytes (RPHs): RPHs were isolated from the livers of SD rats by following previous protocols [25]. After being isolated, the cells were suspended in plating medium and incubated in 96-well plates. Four hours later, when cells had adhered to the plates completely, the medium was replaced with feeding medium containing the corresponding compounds. Another 24 h later, the cell viability and intracellular ROS level were assayed.

Bone marrow-derived macrophages (BMDMs): BMDMs were isolated from the hind legs of mice and were maintained in DMEM supplemented with glucose, 10% FBS, and 15% L929 cell supernatant for ~7 days. Subsequently, the adherent BMDMs were digested and suspended in DMEM supplemented with glucose and 10% FBS. The cells were diluted to a density of 0.5×10^6 cells/mL, and 0.5 mL of the cell suspension was added to one well of a 24-well plate. Twenty-four hours later, the BMDMs were stimulated with LPS (1 μg/mL) or LPS plus the corresponding compounds. The supernatants of the BMDMs were collected 6 or 24 h later for the detection of NO or cytokine (TNF-α, and IL-6) levels.

Animals

All animal experiments in this study were approved by the Institutional Animal Care and Use Committee of Shanghai Institute of Materia Medica, Chinese Academy of Sciences. Male ICR mice (weight: 20–24 g) and SD rats (weight: 200–250 g) were purchased from the Shanghai Slac Laboratory Animal Co., Ltd. (Shanghai, China). All animals were treated humanely and housed in air-conditioned animal quarters. The environment was maintained at a controlled temperature (23 ± 1.5 °C) and humidity (70% ± 20%). The mice had free access to normal food and water.

Cell counting assay

A Cell Counting Kit 8 (CCK 8) was purchased from Yeasen Biotech Co., Ltd. (Shanghai, China). Cells in a 96-well plate were incubated with the corresponding reagents for the indicated time; then, 10 μl of CCK 8 was added to each well and the plate was incubated at 37 °C for 2 h. The absorbance was measured by an automatic microplate reader (Biotek, Winooski, VT, USA) at a wavelength of 450 nm.

DPPH radical scavenging activity

The purple anhydrous ethanol solution of DPPH (0.2 mM) shows maximal absorbance at 510 nm. When DPPH is scavenged by antioxidant substances, the optical density (OD) at 510 nm is reduced. The amount by which the OD_{510 nm} is reduced is linearly correlated with the antioxidative capacity of the compound. The tested compounds, silymarin and the positive control (Vc), were all administered at a concentration of 100 μM and mixed with DPPH for 30 min. The absorbance was measured at a wavelength of 510 nm.

ROS assay

2',7'-Dichlorodihydrofluorescein diacetate (DC-FHDA; Sigma-Aldrich, St. Louis, MO, USA) is usually used for the detection of intracellular ROS. Cells in a 96-well plate were incubated with the corresponding reagents; then, 10 μl of DC-FHDA (10 μM) was added to each well and the plate was incubated for 30 min. DC-FHDA is hydrolyzed to dichlorodihydrofluorescein (DCFH), which is then oxidized to the fluorescent substance dichlorofluorescein (DCF), in cells. The fluorescence intensity of DCF was measured at

excitation and emission wavelengths of 485 nm and 530 nm. The ROS level was calculated as the fold induction relative to the negative control group.

Measurement of NO and cytokine levels

Commercial kits used for the measurement of NO were purchased from Beyotime Biotechnology (Shanghai, China). ELISA kits for the measurement of mouse TNF- α and IL-6 were purchased from Multi Science (Lianke) Biotech. Co., Ltd. (Hangzhou, Zhejiang, China). The NO assay was conducted using the supernatants of BMDMs. The TNF- α and IL-6 levels were analyzed in cell supernatants of BMDMs and mouse serum from the CCl₄ model. All operations were performed in strict accordance with the Manufacturer's instructions. Finally, the OD at a wavelength of 540 nm was detected to quantify the levels of NO, and 450 nm was detected to quantify the levels of TNF- α and IL-6.

Pharmacokinetics study

Plasma was collected from the ICR mice at 5 min, 15 min, 30 min, 1 h, 2 h, 4 h, 8 h, and 24 h after intragastric and intravenous administration (40 mg/kg and 10 mg/kg, respectively). The plasma samples were subjected to centrifugation at 8000 rpm for 10 min and then stored at -80 °C for further study. Mouse liver tissues were collected 15 min, 1 h, 4 h, and 24 h after gigantol administration and stored at -80 °C for further analysis. The concentrations of gigantol in the serum and livers were detected by the LC/MS-8030 triple quadrupole system (Shimadzu Corp., Kyoto, Japan). The negative electrospray ionization interface mode was chosen. Gigantol and the internal standard (glyburide) were separated by ACE C18 columns (100 mm \times 2.1 mm, i.d. 3 μ m). The precursor and product ion values were m/z 273.10 (Q1) $>$ m/z 121.00 (Q3) for gigantol and m/z 492.20 (Q1) $>$ m/z 170.10 (Q3) for glyburide, both with a collision energy of 25 eV. The mobile phase (MP) consisted of acetonitrile (A) and distilled water (C) with a gradient elution of 70% MPC at 0–1 min, 10% MPC at 1–2 min, and 70% MPC at 2.1–6.5 min, at a flow rate of 0.25 mL/min. The oven temperature was 40 °C, and the injection volume was 20 μ L.

Pharmacokinetic parameters

The pharmacokinetic parameters of gigantol were calculated by noncompartmental analysis (NCA) using WinNonlin 6.2 software (Pharsight, Cary, NC). The peak concentration (C_{max}) and the peak time (T_{max}) in the plasma and liver were determined according to the observed data. The areas under the curve (AUCs) from dosing time to the last measurable time (AUC_{0-t}) or extrapolated to infinity ($AUC_{0-\infty}$) were calculated according to the trapezoidal rule. Other parameters, including terminal half-life ($t_{1/2}$), apparent total body clearance (CL/F), mean residence time (MRT), and apparent volume of distribution (Vd/F), were all determined by following a previously described algorithm [26]. The oral bioavailability (F) was calculated according to the following equation: $F (\%) = (AUC_{po} \times Dose_{iv}) / (AUC_{iv} \times Dose_{po}) \times 100\%$.

CCl₄-induced liver injury

After one week of acclimation, all ICR mice were randomly divided into the following seven groups ($n = 6$): vehicle; gigantol alone (40 mg/kg); CCl₄; CCl₄ + bicyclol (200 mg/kg); and CCl₄ + gigantol (10, 20, and 40 mg/kg). The mice were orally administered bicyclol for 3 days and gigantol for 7 days. The mice in the vehicle and CCl₄ groups were administered solvent (0.5% Tween 80). One hour after the last administration, all mice except those in the vehicle and gigantol alone groups were subcutaneously injected with olive oil containing 0.5% CCl₄. Serum and liver samples were collected 16 h later. Serum was obtained from whole blood centrifuged at 8000 rpm for 10 min. Liver tissues were frozen in liquid nitrogen or preserved in formaldehyde solution.

Biochemical analysis

The enzymatic activity of ALT, AST, and LDH was analyzed by a SYSME X JCA-BM6010C automatic clinical analyzer (Kobe, Japan) in the laboratory of the Chinese National Compound Library. The relevant detection kits were purchased from Sysmex Co., Ltd. (Wuxi, Jiangsu, China).

Histopathological and immunohistochemical observations

The fixed liver lobes preserved in 4% formaldehyde were embedded in paraffin and sliced into 3 μ m-thick sections. The sections were stained with hematoxylin and eosin (H&E) and evaluated for pathological changes. Images of all stained slices were visualized and captured by an Olympus CX23 light microscope (Tokyo, Japan). For IHC, the liver sections were deparaffinized, and the antigens were recovered by citrate buffer treatment. After being washed, the liver sections were blocked with goat serum and then stained with a primary antibody against component C9 (OmnimAbs, Alhambra, CA, USA) at 4 °C overnight. Then, the liver sections were incubated with a goat anti-rabbit IgG secondary antibody and detected with a SAB-CHRP kit (Beyotime, Shanghai, China). The IHC images were visualized and captured with a virtual slide scanner Hamamatsu Nanozoomer 2.0 HT (Hamamatsu, Shizuoka prefecture, Japan).

Measurement of lipid peroxidation and total superoxide dismutase

A liver tissue fraction was cut to prepare a 10% homogenate by adding 10 volumes of ice-cold saline. The homogenate was centrifuged at 10,000 rpm and 4 °C for 15 min, and the supernatant was collected for subsequent malondialdehyde (MDA) and total superoxide dismutase (SOD) analyses. Commercial kits used for the measurement of MDA and SOD were purchased from Beyotime Biotechnology (Shanghai, China). The OD at wavelengths of 532 nm and 450 nm was detected to quantify the levels of MDA and SOD, respectively.

Sample preparation and label-free proteomics

Mouse livers from the vehicle, CCl₄ and CCl₄ + gigantol (40 mg/kg) groups were subjected to proteomics analysis. Liver samples were lysed in lysis buffer (4% SDS, 100 mM Tris pH 8.5) and homogenized using Tissue Lyser (BiHeng Biotech, Shanghai, China). Samples were then heated for 10 min at 95 °C and centrifuged at 14,000 $\times g$ for 30 min to collect the supernatant. The proteins were precipitated with cold acetone overnight and redissolved in resuspension buffer (100 mM ammonium bicarbonate, 100 mM Tris pH 8.5, 10% 2,2,2-trifluoroethanol, 10 mM tris(2-carboxyethyl)-phosphine, 40 mM 2-chloroacetamide). The samples were incubated at 50 °C for 10 min and then digested overnight with trypsin (Promega, Madison, WI, USA). Following digestion, the peptides were subjected to vacuum centrifugation drying and C18 solid-phase extraction desalting. The obtained samples were loaded on a self-packed column (75 μ m \times 150 mm, 1.9 μ m ReproSil-Pur C18 beads, Dr. Maisch GmbH, Ammerbuch-Entringen, Germany) and separated with an EASY-nLC 1000 HPLC system (Thermo Fisher Scientific, Waltham, MA, USA) coupled to an MS (Orbitrap Q Exactive, Thermo Fisher Scientific). Peptides were introduced onto the column with buffer A (0.1% formic acid) and eluted with a 180 min gradient of 2%–90% buffer B (100% acetonitrile 0.1% formic acid).

Analysis of the proteomics data

The raw MS spectra were processed using MaxQuant version 1.6.0.1 by searching against the UniProt Mouse database. The false discovery rate was set to 0.01 for both peptide and protein identification. Carbamidomethyl cysteine was searched as a fixed modification. Oxidized methionine and protein N-terminal acetylation were set as variable modifications. Enzyme specificity was

set as trypsin/P. The maximum missing cleavage site was set as 2. The label-free quantification intensity values were used for the subsequent data analysis.

Further bioinformatics analyses were conducted in Microsoft Excel and R statistical computing software. One-way analysis of variance (ANOVA) and the Tukey's honestly significant difference (HSD) test were performed with the R language; [fold change] >1.5 and $P < 0.05$ were set as the criteria for significant changes between any of the two groups. The transformed protein intensity profiles were then clustered by the fuzzy C method using the M fuzz package in R [27]. The optimal number of clusters 'c' and fuzzification parameter 'm' were 4 and 2, respectively, using a Euclidean distance metric. A functional enrichment analysis of the Gene Ontology (GO) of biological processes was performed using the STRING database, and the Kyoto Encyclopedia of Genes and Genomes (KEGG) pathways were analyzed and visualized with the R package Cluster Profiler [28].

RNA extraction and real-time PCR analysis

Total RNA was extracted from the mouse liver using TRIzol reagent (Life Technology, CA, USA) and purified with EZ-10 spin columns and collection tubes (Sangon Biotech, Shanghai, China). Then, the RNA was diluted to the same concentration and reverse transcribed into cDNA with PrimeScriptTM RT Master Mix (Takara, Shiga, Japan). Subsequently, quantitative PCR was performed by mixing template cDNA, forward and reverse primers, and Hieff[®] qPCR SYBR Green Master Mix (Low Rox Plus) (Yeasen Biotech, Shanghai, China). Primers for the target genes and the internal reference gene in the mouse liver are listed in Supplementary Table S2 and Table S3.

Immunofluorescence staining

Fresh mouse liver samples were embedded with optimum cutting temperature compound (O.C.T compound) and sectioned at 10 μm . The slices were stained with antibodies against membrane attack complex C5b-9 (Santa Cruz, Dallas, TX, USA). The primary antibody (dilution 1:100) was applied to the slices and incubated at 4 °C overnight. Subsequently, the sections were washed with phosphate-buffered saline (pH = 7.2) and incubated with an Alexia Fluor 488[®] secondary antibody (Invitrogen, Waltham, MA, USA) for C5b-9. The dilution ratio for secondary antibodies was 1:1000, and the incubation time was 1 h at room temperature. Before being photographed, the slices were sealed with antifade mounting medium containing DAPI (Beyotime Biotech, Shanghai, China). Photomicrographs were taken with an FV1000 MPE confocal microscope (Olympus, Tokyo, Japan) using FV10-ASW software.

Statistical analysis

All the data were analyzed by GraphPad Prism 7.0 software (GraphPad Software Inc., La Jolla, CA, USA) and are shown as the mean \pm SD unless otherwise stated. One-way analysis of variance (ANOVA) was used to compare the differences between more than three groups. $P < 0.05$, $P < 0.01$, and $P < 0.001$ represent significant differences with increasing significance.

RESULTS

(Dihydro-)Stilbene or (dihydro-)phenanthrene derivatives protect hepatocytes against LCA toxicity and exert antioxidative/anti-inflammatory effects in vitro

An in vitro screening platform was established to evaluate the potential effect of (dihydro-)stilbene or (dihydro-)phenanthrene derivatives extracted from *P. chinensis* on liver injury. Thirty-one compounds were assessed in this study. The hepatocyte survival rate, DPPH scavenging activity, and NO inhibition rate were measured (Fig. 1, Supplementary Table S1). These

compounds were ranked based on the results of each assay, with the assays being given identical index weights according to the subjective weight determination method [29] (Supplementary Table S1). Gigantol showed the highest scores of the tested compounds. In the first assay, hiHeps were employed to evaluate the protective effects of the compounds against hepatocyte toxicity induced by LCA. The results showed that 13/31 of the compounds significantly reduced the cell death induced by LCA toxicity at 10 μM (Fig. 1a). Gigantol was the most effective compound, increasing the cell viability by 61% (Supplementary Table S1). In addition, more than 80% of the compounds (100 μM) had a much greater DPPH radical scavenging ability than silymarin (100 μM) (Fig. 1b). Gigantol was the most potent antioxidative compound (DPPH radical scavenging activity \approx 88%) (Supplementary Table S1). LPS-exposed BMDMs were employed to test the anti-inflammatory effect of the compounds. Fifteen of the thirty-one compounds (10 μM) significantly inhibited NO release by BMDMs (Fig. 1c), and the inhibition rate of gigantol was \approx 47% (Supplementary Table S1). No test compounds were found to be toxic to hiHeps at the tested concentrations, whereas three compounds (YS14, YS16, and YS21) significantly affected the viability of BMDMs (Supplementary Fig. S2). The results above indicated that dihydro-stilbene gigantol had better in vitro efficacy than the other components and should be further investigated.

Gigantol reduces cell death and oxidative stress in hepatocytes

Here, the dose-dependent effects of gigantol (Fig. 2a) on hepatocytes were detected in both hiHeps and rat primary hepatocytes (RPHs). Gigantol at concentrations below 250 μM did not affect the viability of hiHeps, and gigantol at a concentration of 250 μM slightly reduced the viability of RPHs (Fig. 2b). Different concentrations of gigantol were added together with LCA at 50 μM or 30 μM to RPHs and hiHeps for 24 h. The cell viability and ROS levels were measured by CCK8 and DCFH-DA, respectively. In both hiHeps and RPHs treated with LCA, gigantol was found to significantly increase viability and reduce ROS levels in a dose-dependent manner (Fig. 2c, d). The minimum effective dose was \approx 0.1 μM . These results suggest that gigantol has a broad safety range in hepatocytes and that its hepatoprotective effect can be attributed to its antioxidation activity.

Anti-inflammatory effect of gigantol on BMDMs stimulated with LPS
NO and pro-inflammatory cytokines such as TNF- α and IL-6 released by Kupffer cells in the liver play an important role in inflammation progression. In this study, we used an LPS-exposed BMDM model to validate whether gigantol had a direct inhibitory effect on macrophage activation. Gigantol did not influence the viability of BMDMs (Fig. 2e). The levels of NO and TNF- α /IL-6 in the supernatant of BMDMs stimulated with LPS were all reduced by gigantol in a dose-dependent manner (Fig. 2f-h). The minimum effective dose was less than 1 μM . These results indicate that gigantol may inhibit the inflammatory response of Kupffer cells during liver injury.

Pharmacokinetics profile of gigantol

To investigate the ADME properties of gigantol, we conducted in vivo pharmacokinetic studies using ICR mice. The mean plasma concentration-time curves and the mean liver concentration-time curves of gigantol are shown in Fig. 3a, 3b. The pharmacokinetic parameters of gigantol were calculated by the noncompartmental model (Table 1). The results indicated that gigantol was absorbed quickly; its plasma concentration peaked 5 min after administration, and its C_{max} values were 230.24 ± 388.21 ng/mL (po) and 808.57 ± 116.48 ng/mL (iv). The $\text{AUC}_{0-24 \text{ h}}$ of gigantol was 39.63 ± 86.35 h*ng/mL (po) and 65.55 ± 10.96 h*ng/mL (iv). The oral bioavailability of gigantol was about 11.5%. The C_{max} and AUC values of gigantol in the liver

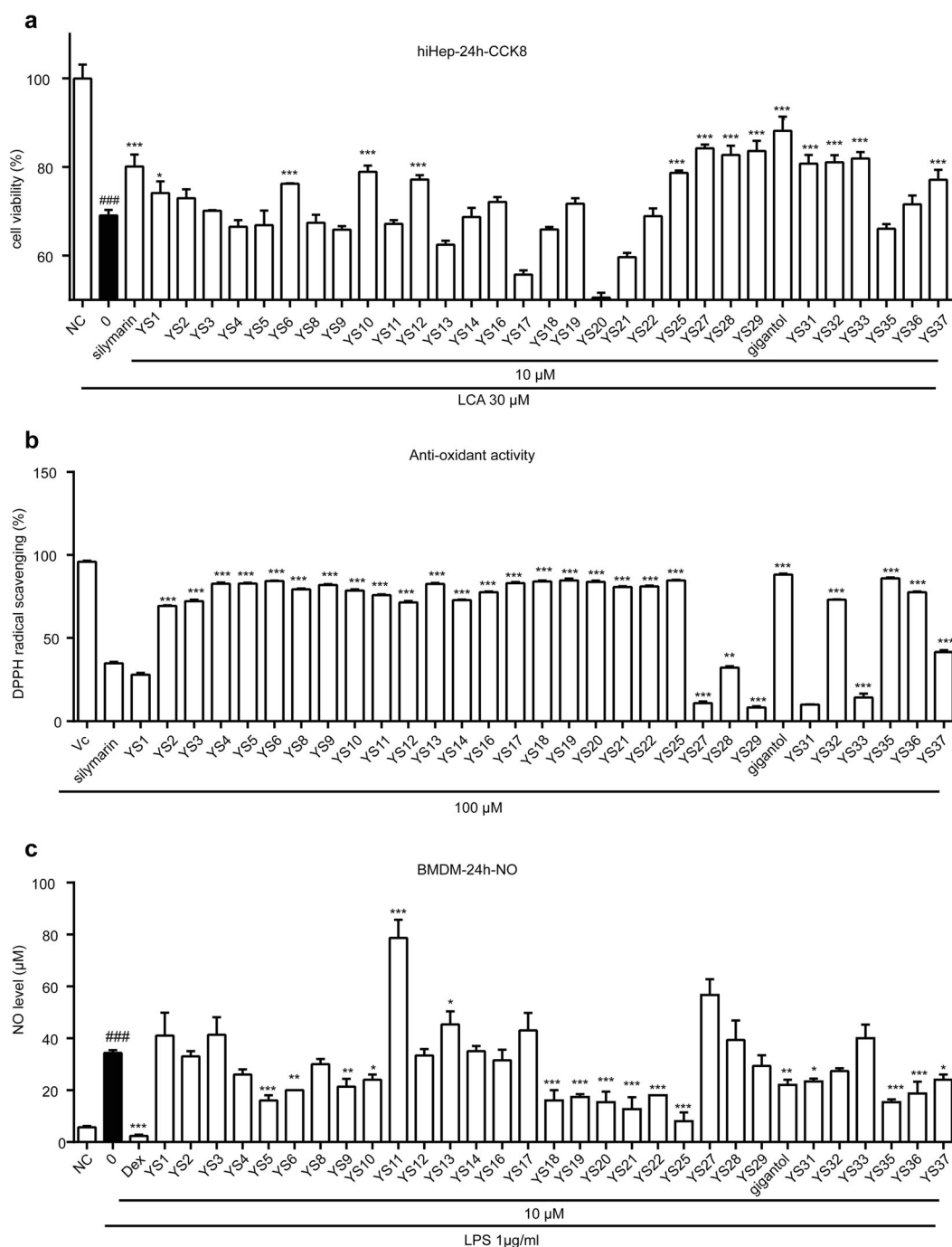


Fig. 1 In vitro biological evaluation of gigantol and its derivatives. The representative results are shown as the mean \pm SD, $n = 3$. **a** Effect of the 31 compounds on LCA toxicity in hiHeps. Silymarin was used as the positive control. $###P < 0.001$ the LCA-induced control vs. the negative control (NC); $*P < 0.05$, $***P < 0.001$ vs. the LCA-treated control. **b** DPPH radical scavenging activity of the compounds. Vc and silymarin were used as positive controls. $**P < 0.01$, $***P < 0.001$ vs. the silymarin group. **c** Effect of the compounds on NO release by BMDMs. Dexamethasone (Dex) was used as a positive control. $###P < 0.001$ the LPS-treated control vs. NC; $*P < 0.05$, $**P < 0.01$, $***P < 0.001$ vs. the LPS-treated control

were also calculated (Table 2). Fifteen minutes after the oral and intravenous administration of gigantol, the liver concentration of gigantol reached 6070.59 ± 1685.39 ng/g protein (po) and 4793.60 ± 1255.03 ng/g protein (iv). The $AUC_{0-24 h}$ values were 14988.73 ± 5165.96 h*ng/g protein (po) and 5707.01 ± 1145.54 h*ng/g protein (iv). The C_{max} and $AUC_{0-24 h}$ values of gigantol in the liver were 26-fold and 375-fold higher, respectively, than those in the plasma. In summary, the moderate oral bioavailability and high level of liver exposure of gigantol indicate that it may be efficacious after oral administration.

Protective effect of gigantol against CCl_4 -induced liver injury
The pharmacodynamic experiments were conducted according to the scheme shown in Fig. 4a. The results revealed that gigantol reduced the levels of ALT, AST, and LDH in the mouse serum in a dose-dependent manner (Fig. 4b–d). In addition, the H&E staining experiments suggested that centrilobular necrosis, tumefaction and steatosis, as well as inflammatory cell infiltration, were all improved by gigantol (Fig. 4e). Overall, these results support our hypothesis that the oral administration of gigantol could prevent liver injury in vivo.

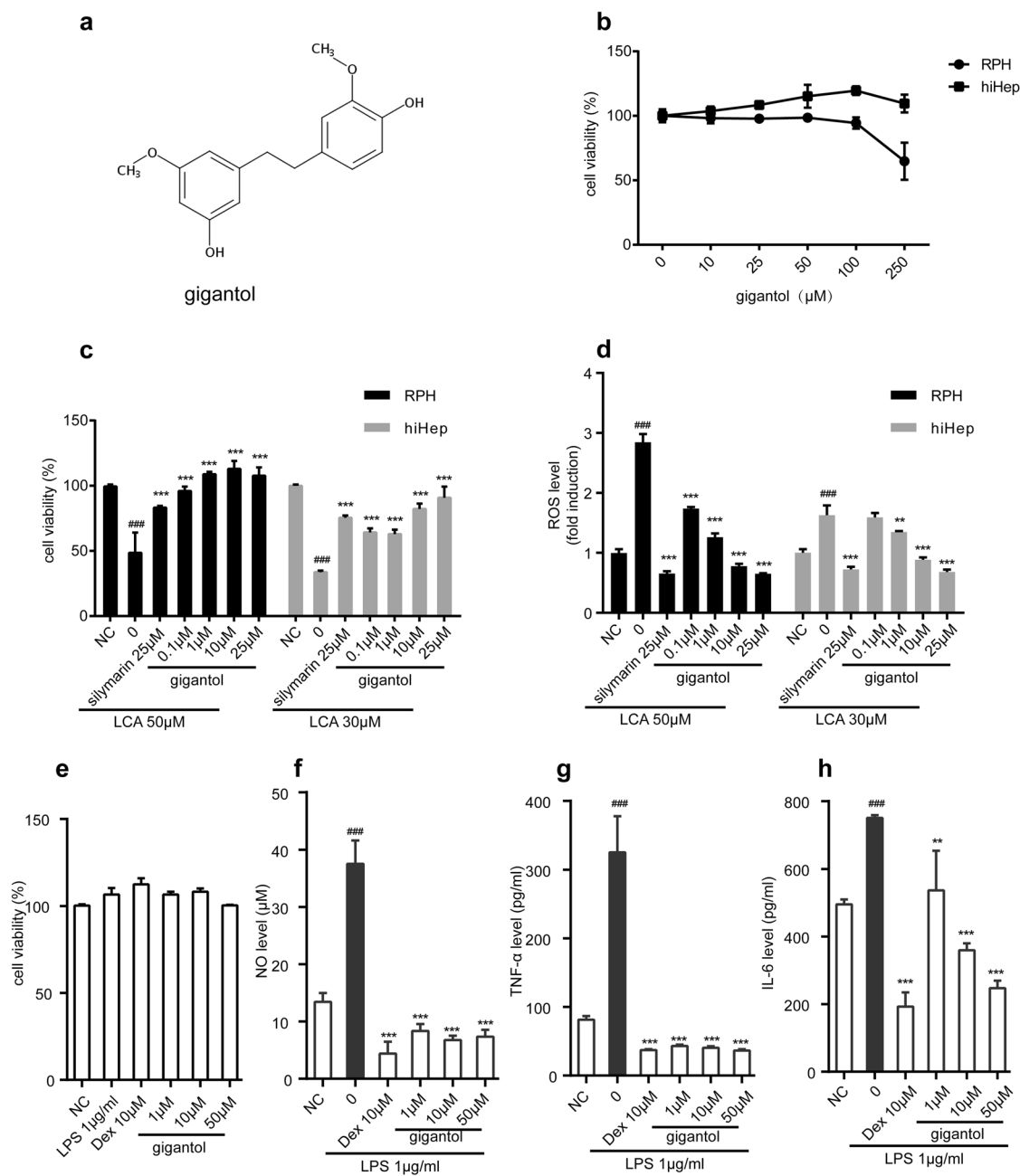


Fig. 2 Gigantol alleviates oxidative stress in hepatocytes and inflammatory responses in BMDMs. **a** The structure of gigantol. **b** The effect of gigantol on the viability of RPHs and hiHeps. The dose-dependent effects of gigantol on the **c** viability and **d** ROS levels in both hiHeps and RPHs treated with LCA. The results are shown as the mean \pm SD, $n = 3$. $###P < 0.001$ the LCA-treated control vs. NC; $**P < 0.01$, $***P < 0.001$ vs. the LCA-induced control. **e** The effects of gigantol, LPS, and Dex on the viability of BMDMs. The inhibitory effects of gigantol on **f** NO, **g** TNF- α , and **h** IL-6 production in BMDMs stimulated with LPS. Representative results are shown as the mean \pm SD, $n = 3$. $###P < 0.001$ the LPS-treated control vs. NC; $**P < 0.01$, $***P < 0.001$ vs. the LPS-treated control

Gigantol reverses liver oxidation and inflammation induced by CCl_4 in mice

Furthermore, we verified the effect of gigantol on liver oxidative stress and inflammatory responses in the CCl_4 -induced liver injury model. The increase in free radicals caused by CCl_4 can induce lipid peroxidation and reduce endogenous antioxidant enzymes in the liver. The MDA content, which was used as an indicator of lipid peroxidation, was dose-dependently reduced by gigantol (Fig. 5a). The level of SOD, an endogenous antioxidant enzyme, was increased by gigantol (Fig. 5b). The levels of pro-inflammatory cytokines and chemokines are known to be increased under inflammatory conditions. Gigantol

dose-dependently decreased the TNF- α and IL-6 levels in the serum (Fig. 5c, d). In addition, the increased mRNA expression of cytokines (TNF- α , IL-6, and IL-1 β) and chemokines (MCP-1 and ICAM-1) was also inhibited by gigantol (40 mg/kg) (Fig. 5e–i). The above results indicate that gigantol significantly relieves oxidative stress and inflammatory responses in the CCl_4 -induced liver injury model.

Proteomic analysis of the potential targets and pathways regulated by gigantol

To uncover the specific hepatoprotective mechanism of gigantol, liver tissues from the vehicle, CCl_4 and CCl_4 + gigantol (40 mg/kg)

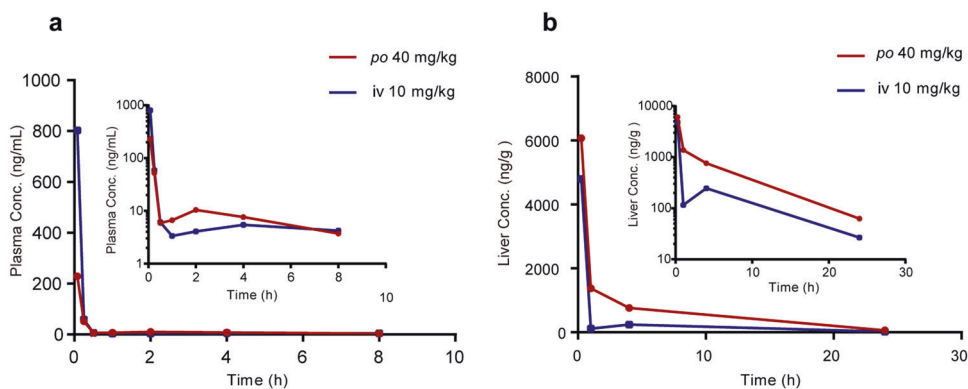


Fig. 3 Concentration of gigantol in the plasma and livers of mice. **a** The mean plasma concentration-time curve and **b** the mean liver concentration-time curve of gigantol after oral (*po*) and intravenous (*iv*) administration. The plasma and liver concentrations of gigantol in the inner figures were converted to logarithmic data

Parameters	<i>po</i> 40 mg/kg	<i>iv</i> 10 mg/kg
$T_{1/2}$ (h)	0.17 ± 0.11	0.060 ± 0.0020
T_{max} (h)	0.083 ± 0.00	
C_{max} (ng/mL)	230.24 ± 388.21	
AUC_{0-t} (h*ng/mL)	39.63 ± 86.35	65.55 ± 10.96
$AUC_{0-\infty}$ (h*ng/mL)	41.98 ± 64.38	86.90 ± 11.05
CL (L·h ⁻¹ ·kg ⁻¹)		116.65 ± 16.55
MRT (h)	0.16 ± 0.046	0.13 ± 0.0094
Vd (L/kg)		10.19 ± 1.40
F (%)	11.47	

Parameters	<i>po</i> 40 mg/kg	<i>iv</i> 10 mg/kg
C_{max} (ng/g)	6070.59 ± 1685.39	4793.60 ± 1255.03
AUC_{0-t} (h*ng/g)	14988.73 ± 5165.96	5707.01 ± 1145.54
$AUC_{0-\infty}$ (h*ng/g)	15569.99 ± 5008.41	6107.51 ± 1210.93

groups were subjected to label-free proteomics analysis (Fig. 6a). A total of 4069 proteins were analyzed, and 497 proteins were found to be significantly regulated by CCl₄ or gigantol ($P < 0.05$ and [fold change] > 1.5). The differentially expressed proteins (DEPs) were assigned to four clusters by a fuzzy *c*-means (FCM) clustering algorithm (Fig. 6b). The protein numbers in cluster 1-cluster 4 were 99, 167, 146, and 85, respectively. Since the expression of the proteins in cluster 1 or cluster 3 was downregulated or upregulated by CCl₄ and significantly reversed by gigantol, we mainly focused on the proteins in these two clusters. GO and KEGG pathway enrichment analyses were used to elucidate the biological processes and relevant pathways of these proteins. The results showed that proteins in cluster 1 were enriched in only one KEGG pathway (spliceosome), and the enriched GO terms were mainly associated with mRNA processing and RNA splicing (Supplementary Fig. S3), which are not directly relevant to oxidative stress or inflammatory responses. Proteins in cluster 3 were enriched in 47 GO terms ($P < 0.05$) and 12 KEGG pathways ($P < 0.05$). Figure 6c shows the top 10 GO terms, among which the immune system process was most significantly reversed by

gigantol (counts = 11, $P = 8.08 \times 10^{-4}$). Accordingly, the top 10 KEGG pathways were listed, and the complement and coagulation cascades were found to be the predominant pathways (counts = 9, $P = 5.01 \times 10^{-7}$) (Fig. 6d).

Terminal complement complex-associated C9 expression is significantly reversed by gigantol
The protein counts in the complement and coagulation cascades were ranked according to the fold change between the CCl₄ group and the CCl₄ + gigantol group (Fig. 6e). The proteins relevant to the complement system are complement component C9 (C9), complement component C8 beta chain (C8β), complement factor D (Cfd), and complement factor H (Cfh). Proteins belonging to the coagulation system include alpha-1-antitrypsin 1-1 (serpina1α), fibrinogen alpha chain (Fga), fibrinogen beta chain (Fgβ), fibrinogen gamma chain (Fgy), and prothrombin (F2). The results showed that the expression of complement component C9 was most notably reversed by gigantol (downregulated fold change = 6.15, $P < 0.01$) (Fig. 6f). The immunohistological staining results of C9 expression corresponded well with the proteomics data. Gigantol significantly decreased the number of C9-positive cells in the livers of mice treated with CCl₄ (downregulated fold change = 4.87, $P < 0.001$) (Fig. 6g, h).

Gigantol inhibits the formation of TCCs induced by CCl₄
Complement component C9 is an important component of the TCC, which contains one molecule of C5b, C6, C7, and C8 and twelve molecules of C9 [30]. TCCs have been reported to insert into the lipid bilayer and form pores in the cell membrane, thus causing ion influx and triggering several pro-inflammatory signaling pathways [22]. We verified the formation of TCCs by detecting the gene expression of several TCC components, as well as C3, which is the precursor of C5b. The results showed that CCl₄ treatment significantly increased the mRNA expression of C3 and TCC components, which were all downregulated by gigantol (Fig. 7a). The gene expression of C9 was increased to the greatest extent by CCl₄ and reversed by gigantol to a baseline level, which is consistent with the proteomics analysis and IHC staining results. Furthermore, we tested the mRNA expression of the TCC regulators CD59a/b (inhibitors of TCC) [31] and hepatic transcription factor hepatocyte nuclear factor 1α/4α (potential activators of TCC) [32, 33]. The gene expression of CD59a and CD59b was reduced by CCl₄, and the expression of only CD59b was upregulated by gigantol (Fig. 7b). CCl₄ also significantly upregulated the expression of Hnf4α, and gigantol pretreatment reduced the expression of both Hnf1α and Hnf4α (Fig. 7b). Moreover, we detected the formation of C5b-9 with the help of confocal microscopy. The results showed that CCl₄ significantly

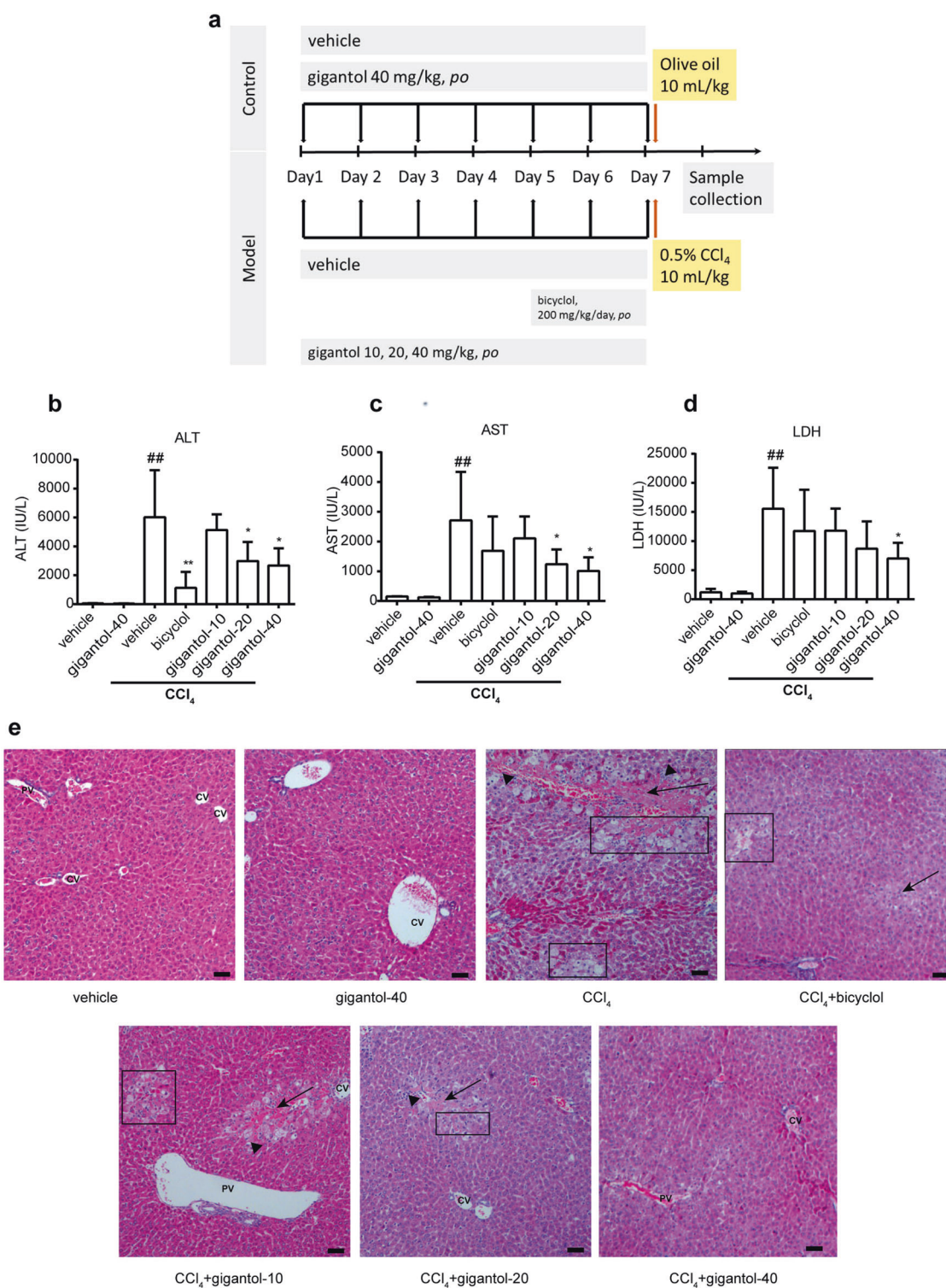


Fig. 4 Protective effect of gigantol on CCl₄-induced acute liver injury. **a** An overview of the experimental scheme. **b** ALT, **c** AST, and **d** LDH levels in mouse serum. The above results are shown as the mean \pm SD, $n = 6$. ^{##} $P < 0.001$ the CCl₄ group vs. the vehicle group; ^{*} $P < 0.05$, ^{**} $P < 0.01$, ^{***} $P < 0.001$ vs. the CCl₄ group. **e** Representative histological sections of liver tissues stained with H&E. Scale bar = 50 μ m. Symbols: black arrow: centrilobular necrosis; rectangle: tumefaction and steatosis; solid triangle: inflammatory cell infiltration; CV centrilobular veins; PV portal veins

increased the localization of C5b-9 around hepatic vessels, which was inhibited by gigantol (Fig. 7c). Overall, these mechanistic studies suggest that the anti-inflammatory effect of gigantol in the liver could be attributable to the inhibition of C5b-9 formation.

DISCUSSION

In this study, a series of (dihydro-)stilbene or (dihydro-)phenanthrene derivatives extracted from *P. chinensis* were identified and screened for their potential hepatoprotective, antioxidant, and anti-inflammatory activity. Gigantol was selected for further studies due

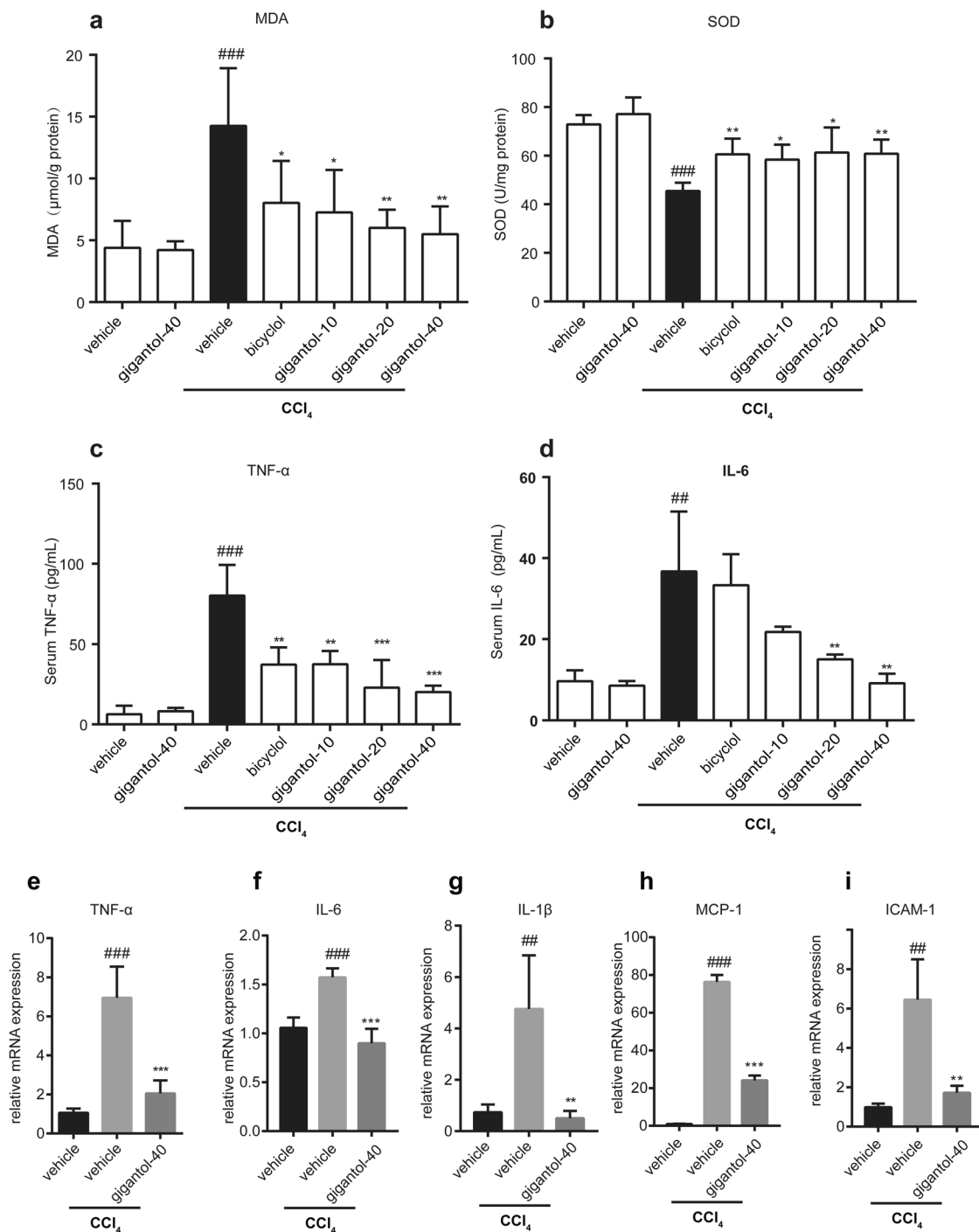


Fig. 5 Role of gigantol in hepatic oxidative stress and inflammation in mice. **a** The MDA and **b** SOD levels in the liver. **c** TNF-α and **d** IL-6 levels in the serum. **e**–**i** The mRNA expression of pro-inflammatory cytokines (TNF-α, IL-6, and IL-1β) and chemokines (MCP-1 and ICAM-1) in the liver. Representative results are shown as the mean ± SD, *n* = 6. ###*P* < 0.01, ###*P* < 0.001 the CCl₄ group vs. the vehicle group; **P* < 0.05, ***P* < 0.01, ****P* < 0.001 vs. the CCl₄ group

to its excellent in vitro efficacy and high level of exposure in mouse livers. We found that the oral administration of gigantol relieved lipid peroxidation and inflammatory responses in the CCl₄-induced liver injury model. Moreover, proteomics analysis along with various biochemical methods were used to explore the potential antioxidative and anti-inflammatory mechanisms of gigantol.

LCA is a hydrophobic bile acid (BA) that can induce hepatocyte injury by disrupting the cell membrane, damaging mitochondria, and producing ROS [34]. According to our previous study, hiHeps

can be used as an alternative to primary human hepatocytes to evaluate the toxicity of cholestatic agents and hydrophobic BAs [24]. In this study, hiHeps were employed to evaluate the effects of the test compounds on LCA-induced cell death and ROS production. The results indicated that gigantol had the strongest protective effect against hepatocyte injury and dose-dependently reversed the LCA-induced effects on cell viability and intracellular ROS level in both hiHeps and RPHs. The in vitro minimum effective dose was ~100 nM. The antioxidant activity was also tested in the

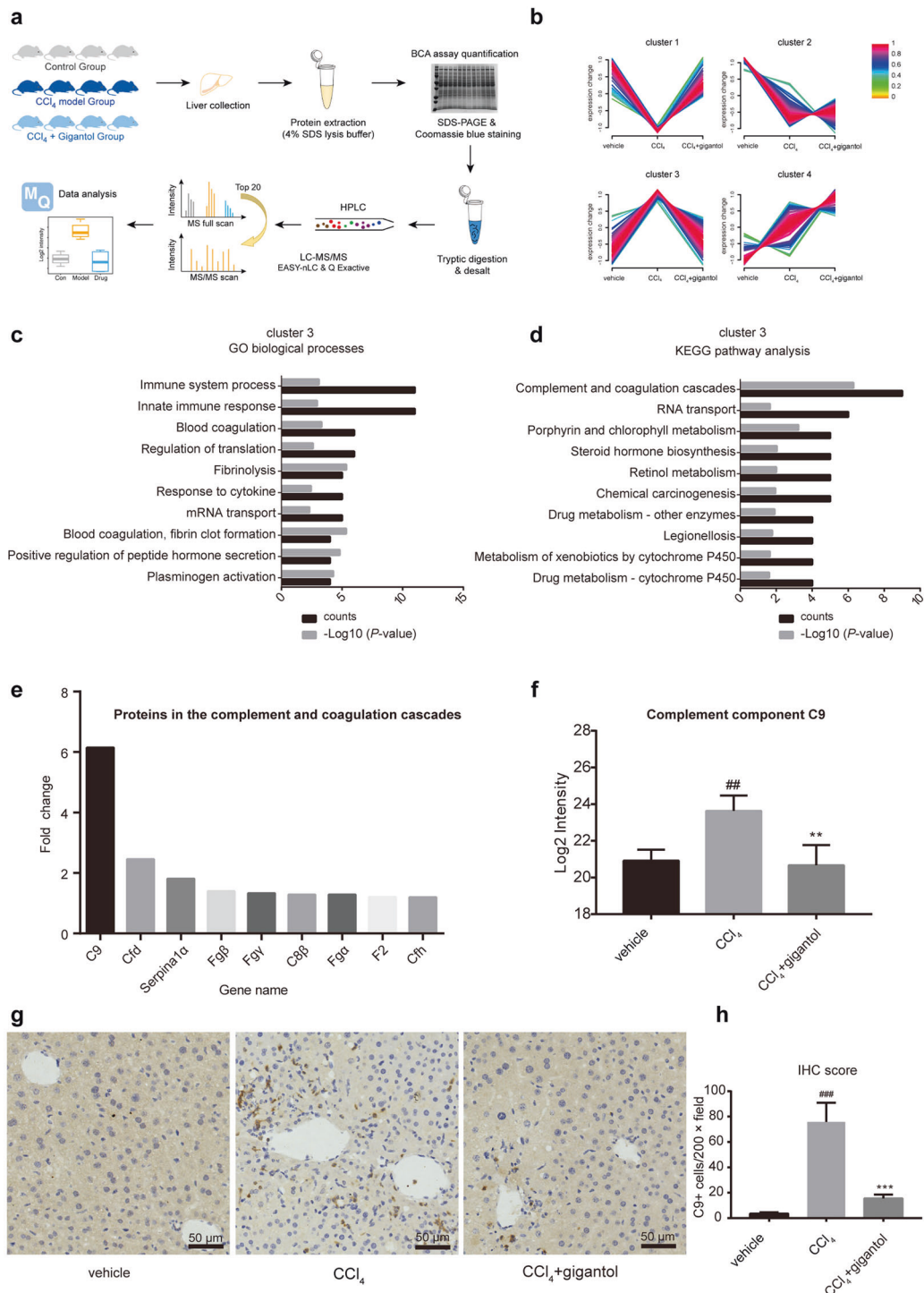


Fig. 6 TCC-associated complement component C9 expression is markedly reduced by gigantol. **a** Schematic of the experimental strategy used to perform label-free proteomics. A total of 4069 proteins were analyzed. **b** Clustering of the differentially expressed proteins (DEPs). The expression of a total of 497 proteins was found to be significantly changed between the vehicle group, CCl₄ group, and CCl₄ + gigantol group. The proteins with altered expression levels were assigned to four clusters by a fuzzy c-means (FCM) clustering algorithm (cluster 1: 99; cluster 2: 167; cluster 3: 146; and cluster 4: 85). The y-axis is log₁₀ transformed and normalized. **c** The GO biological analysis and **d** KEGG pathway analysis of the proteins in cluster 3. **e** Fold changes of proteins in the complement and coagulation cascades. **f** The relative level of the C9 protein in different groups according to the proteomics analysis. **g** Representative images of immunohistological staining showing C9 expression in the livers of mice. **h** The quantitative results of the C9⁺ cell numbers in mouse livers. The results are shown as the mean ± SD, *n* = 6. ##*P* < 0.01, ###*P* < 0.001, the CCl₄ group vs. the vehicle group; ***P* < 0.01, ****P* < 0.001 vs. the CCl₄ group

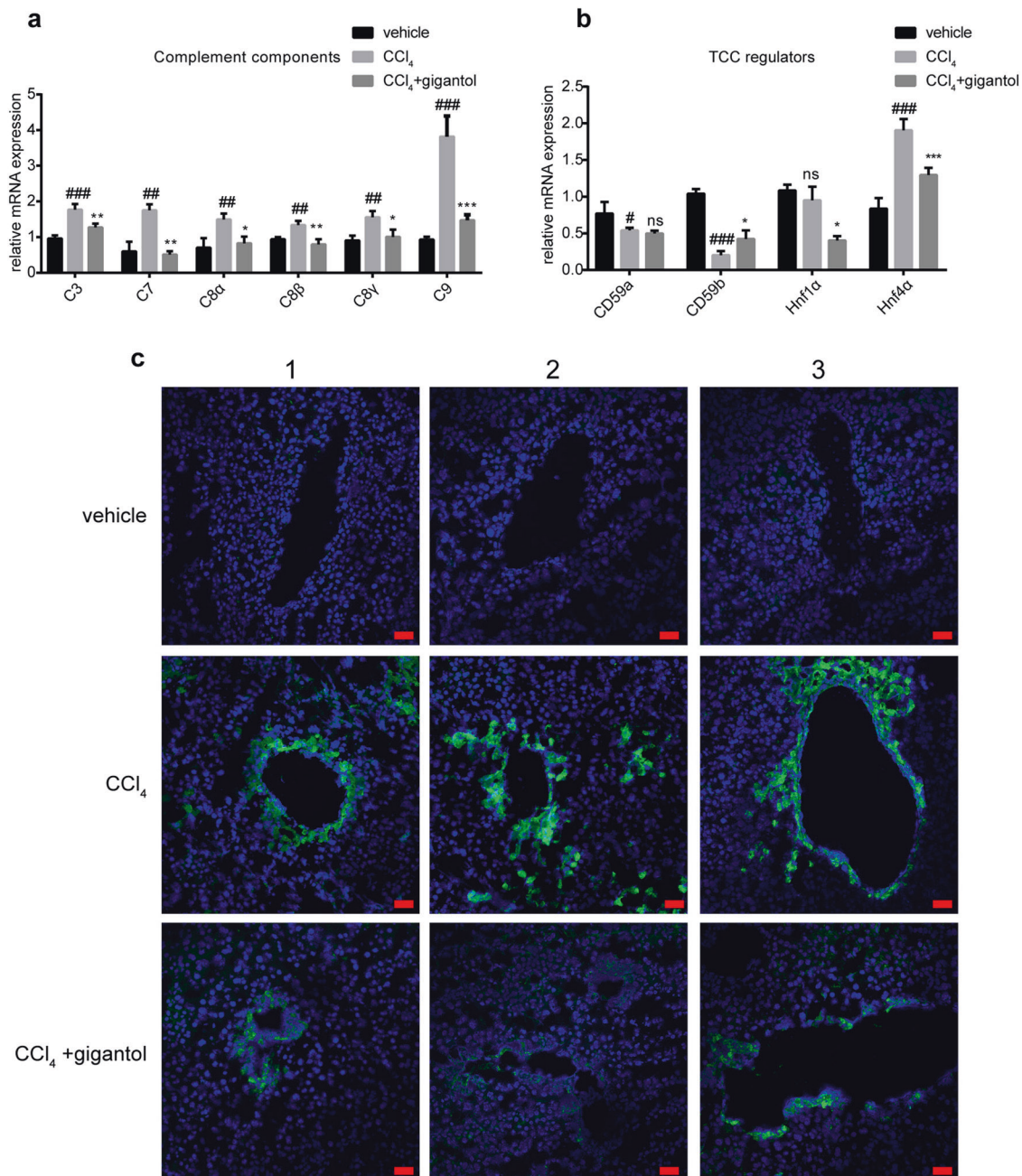


Fig. 7 Gigantol reduces TCC (C5b-9) formation in mouse livers. **a** The relative mRNA expression of the components in the early and terminal complement systems in mouse livers. **b** The relative mRNA expression of TCC regulators in mouse livers. The results are shown as the mean \pm SD; $n = 6$. # $P < 0.05$, ## $P < 0.01$, ### $P < 0.001$ the CCl₄ group vs. the vehicle group; * $P < 0.05$, ** $P < 0.01$, *** $P < 0.001$ vs. the CCl₄ group; ns indicates a nonsignificant difference. **c** Immunofluorescence staining of TCC in mouse livers. Three of the representative merged images of TCC (green) and DAPI (blue) in each group are displayed. Scale bar = 50 μ m

DPPH radical scavenging experiment. The radical scavenging rate of gigantol was the greatest, ~88%.

The inflammatory response is a complex process involving inducers (pathogen- and damage-associated molecular patterns (PAMPs and DAMPs)) [35], sensors (e.g., Kupffer cells and neutrophils) [36], and pro-inflammatory mediators (e.g., TNF- α , IL-6, and ROS). Our results indicate that gigantol reduces DAMP release by scavenging oxygen radicals and preventing cell death and directly blocking PAMP (LPS) stimulation in macrophages. In the BMDM study, gigantol significantly inhibited the release of NO, TNF- α , and IL-6. These results suggest that gigantol may have the ability to alleviate liver inflammation in vivo.

Considering the encouraging in vitro data, we performed in vivo studies to investigate the pharmacokinetics of gigantol in ICR mice. The pharmacokinetic parameters showed that gigantol had a short half-life in mice and that the bioavailability was ~11.5%. Strikingly, the C_{max} and $AUC_{0-24\text{ h}}$ values of gigantol in the liver were 26-fold and 375-fold higher, respectively, than those in the plasma, which partially indicates its oral hepatoprotective efficacy.

Since gigantol has strong ROS scavenging activity and cytokine inhibition effects, mouse liver injury induced by CCl₄ was used for further research. The pathogenesis of this animal model involves early oxidative stress and subsequent fulminant inflammation [37], which was expected to be reversed by gigantol. In the CCl₄-

induced liver injury model, gigantol gavage for seven continuous days reduced the levels of serum biomarkers (ALT, AST, and LDH) and liver pathological alterations. Lipid peroxidation and inflammatory responses were also attenuated by gigantol. Compared with that of the positive control (bicyclol), the inhibitory effect of gigantol on the serum ALT level was consistent with its effect on the AST and LDH levels. At a dosage of $40 \text{ mg} \cdot \text{kg}^{-1} \cdot \text{d}^{-1}$, gigantol significantly improved ALT, AST, and LDH levels, while bicyclol significantly improved only ALT levels, which is consistent with the findings of a previous report [38]. The effect of another positive control, silymarin, on CCl_4 -induced liver injury was also studied but it was not efficacious via intragastric administration (data not shown). To some extent, these phenomena suggest that gigantol may have better oral efficacy than bicyclol and silymarin.

To investigate the potential targets and molecular mechanisms underlying the antioxidative and anti-inflammatory effects of gigantol, mouse livers from the vehicle, CCl_4 , and CCl_4 + gigantol groups were subjected to label-free proteomics analysis. The 497 DEPs were assigned to four clusters, and proteins in cluster 1 and cluster 3 were further subjected to GO biological process analysis and KEGG pathway analysis. We found that proteins in cluster 3 were highly relevant to immune system processes, innate immune responses, and blood coagulation. Correspondingly, the complement and coagulation cascades were enriched in the KEGG pathway analysis with the highest gene counts and lowest *P* values.

The liver is responsible for the production of 80%–90% of the complement proteins and expresses several complement receptors. Conversely, the complement system is involved in the pathogenesis of various liver disorders [39]. Increased C3a, C5a, and C5b-9 deposition in the liver has been found in liver injury caused by viral hepatitis [40], trichloroethylene (TCE) [41, 42], LPS/D-GalN injection [43], and I/R [44]. A lack of C3 in mice alleviates the hepatic steatosis induced by ethanol, and C5 deficiency contributes to lower serum alanine aminotransferase and reduces TNF- α and IL-6 levels [45, 46]. A clinical study revealed that NASH is more prevalent in patients with increased hepatic C9 deposition, which leads to increased levels of neutrophil infiltration and cytokines in the liver [47]. In addition, the activation of the complement system is often accompanied by the activation of the coagulation system during tissue damage and inflammatory responses [48]. Our results show that gigantol markedly reverses the increased expression of complement component C9 (C9), complement component C8 beta chain (C8 β), complement factor D (Cfd), and complement factor H (Cfh). Gigantol inhibited the activation of the coagulation system by downregulating the expression of serpin1a, Fga, Fg β , Fgy, and F2. Among these, the fold change of C9, which has been proposed to be a potential target for gigantol, was the most significant between the CCl_4 model and gigantol pretreatment groups. The protein and gene expression of C9 were further validated by immunohistological staining and RT-PCR. C9 is an important component of the TCC (C5b-9), which contains one molecule of C5b, C6, C7, and C8 and 12 molecules of C9 [30]. TCCs have been reported to insert into the lipid bilayer and form pores in the cell membrane, thus causing ion influx and triggering several pro-inflammatory signaling pathways [22]. In addition to that of C9, the increased mRNA expression of other TCC components was also significantly reversed by gigantol. In our study, the immunofluorescence staining results showed that CCl_4 treatment significantly increased the vascular deposition of TCCs in the liver, which was significantly inhibited by gigantol pretreatment. These results imply that the anti-inflammatory effect of gigantol is closely associated with the inhibition of C5b-9.

In addition, the mRNA expression of TCC regulators was also regulated by gigantol. CD59 is a membrane complement

inhibitory protein that can interfere with the formation of TCCs by preventing the recruitment of C9 to the C5b-8 complex [49]. Our study indicates that CCl_4 significantly reduces the gene expression of CD59b, which promotes the binding of C9 to C5b-8. Gigantol increased the gene expression of CD59b, thus inhibiting the formation of TCCs. Hnf1 α has been reported to be a positive regulator of the gene expression of TCC components, including C5, C8 α , C8 β , C8 γ , and C9 [32]. Hnf4 α has been reported to potentially activate the transcription of C3 [33] and the complement factor B gene [50], which are also important constituents of complement activation. Our results show that gigantol reduces the gene expression of these two hepatocyte nuclear factors, which is consistent with the downregulated gene expression of complement components.

During the past few decades, TCC has been suggested as a pro-inflammatory trigger, and TCC inhibition is hypothesized to be an anti-inflammatory strategy for many diseases [22], including liver inflammation. For example, CD59 deficiency leads to increased TCC deposition in mice, thus exacerbating I/R-induced liver injury [51]. However, liver dysfunction in this model is ameliorated by C6 deficiency in rats [52]. The protective effect of TCC inhibition on I/R-induced liver injury has also been proven by the site-targeting murine fusion protein CR2-CD59, which specifically inhibits the assembly of TCCs and alleviates liver injury [44]. Considering that the early complement pathways also play important roles in liver regeneration and the maintenance of innate immune defenses against infection [53], specific TCC inhibition could be a safer and more effective therapeutic for protecting against liver injury. Some small molecules have also been reported to be TCC blockers but have not been applied in liver injury [54]. This is the first report of a small molecule as a potential TCC inhibitor that exerts a protective effect against liver inflammation. In future studies, more assays should be conducted to determine whether gigantol is a specific TCC blocker and its applicability to other liver diseases, such as NASH.

In summary, the dihydro-stilbene gigantol was found for the first time to prevent hepatic oxidative stress and inflammation both *in vitro* and *in vivo*. Our study highlights the importance of TCC-associated C9 in the pathogenesis of liver inflammation induced by CCl_4 . Gigantol may be a promising drug candidate for acute or chronic liver injury and acts via a novel mechanism of inhibiting C5b-9 formation in the liver.

ACKNOWLEDGEMENTS

This study was supported by the 'Organ Reconstruction and Manufacturing' Strategic Priority Research Program of the Chinese Academy of Sciences [grant number XDA16020205], the National Science Foundation of China [grant number 81872927], the International Partnership Program of Chinese Academy of Sciences [grant number 153631KYSB20160004], the Independent Deployment Program of the Institute of Pharmaceutical Innovation of the Chinese Academy of Sciences [grant number CASIMM0120184005], and the China Postdoctoral Science Foundation [grant number 2019M651623].

AUTHOR CONTRIBUTIONS

YRX, GYP, SY and YY designed the research; YRX and GYP wrote the paper; YRX, QL, ZLP, QQD, BL, SY, and ZHM conducted the experiments; YRX, QL, and ZLP were responsible for the data analysis; SY, QL, LW, and HZ helped revise the paper. All the authors reviewed and agreed on the final version.

ADDITIONAL INFORMATION

The online version of this article (<https://doi.org/10.1038/s41401-020-0406-6>) contains supplementary material, which is available to authorized users.

Competing interests: The authors declare no competing interests.

REFERENCES

- de Andrade KQ, Moura FA, dos Santos JM, de Araujo OR, de Farias Santos JC, Goulart MO. Oxidative stress and inflammation in hepatic diseases: therapeutic possibilities of N-acetylcysteine. *Int J Mol Sci.* 2015;16:30269–308.
- Diesen DL, Kuo PC. Nitric oxide and redox regulation in the liver: part I. General considerations and redox biology in hepatitis. *J Surg Res.* 2010;162:95–109.
- Diesen DL, Kuo PC. Nitric oxide and redox regulation in the liver: part II. Redox biology in pathologic hepatocytes and implications for intervention. *J Surg Res.* 2011;167:96–112.
- Asrani SK, Devarbhavi H, Eaton J, Kamath PS. Burden of liver diseases in the world. *J Hepatol.* 2019;70:151–71.
- Wendel A, Feuerstein S. Drug-induced lipid peroxidation in mice-I. Modulation by monooxygenase activity, glutathione and selenium status. *Biochem Pharmacol.* 1981;30:2513–20.
- Singh R, Czaja MJ. Regulation of hepatocyte apoptosis by oxidative stress. *J Gastroenterol Hepatol.* 2007;22(Suppl 1):S45–8.
- Hong JY, Lebofsky M, Farhood A, Jaeschke H. Oxidant stress-induced liver injury in vivo: role of apoptosis, oncotic necrosis, and c-Jun NH₂-terminal kinase activation. *Am J Physiol Gastrointest Liver Physiol.* 2009;296:G572–81.
- Jaeschke H. Reactive oxygen and mechanisms of inflammatory liver injury. *J Gastroenterol Hepatol.* 2000;15:718–24.
- Santos JC, Valentim IB, de Araujo OR, Ataíde Tda R, Goulart MO. Development of nonalcoholic hepatopathy: contributions of oxidative stress and advanced glycation end products. *Int J Mol Sci.* 2013;14:19846–66.
- Rumack BH, Peterson RC, Koch GG, Amara IA. Acetaminophen overdose. 662 cases with evaluation of oral acetylcysteine treatment. *Arch Intern Med.* 1981;141:380–5.
- Wang AL, Wang JP, Wang H, Chen YH, Zhao L, Wang LS, et al. A dual effect of N-acetylcysteine on acute ethanol-induced liver damage in mice. *Hepatol Res.* 2006;34:199–206.
- Atkinson MC. The use of N-acetylcysteine in intensive care. *Crit Care Resusc.* 2002;4:21–7.
- Zhao J, Agarwal R. Tissue distribution of silybinin, the major active constituent of silymarin, in mice and its association with enhancement of phase II enzymes: implications in cancer chemoprevention. *Carcinogenesis.* 1999;20:2101–8.
- Wu JW, Lin LC, Tsai TH. Drug-drug interactions of silymarin on the perspective of pharmacokinetics. *J Ethnopharmacol.* 2009;121:185–93.
- Wu JW, Lin LC, Hung SC, Chi CW, Tsai TH. Analysis of silybinin in rat plasma and bile for hepatobiliary excretion and oral bioavailability application. *J Pharm Biomed Anal.* 2007;45:635–41.
- Farrell GC, Haczeyni F, Chitturi S. Pathogenesis of NASH: how metabolic complications of overnutrition favour lipotoxicity and pro-inflammatory fatty liver disease. *Adv Exp Med Biol.* 2018;1061:19–44.
- Domitrovic R, Potocnjak I. A comprehensive overview of hepatoprotective natural compounds: mechanism of action and clinical perspectives. *Arch Toxicol.* 2016;90:39–79.
- Lam Y, Ng TB, Yao RM, Shi J, Xu K, Sze SC, et al. Evaluation of chemical constituents and important mechanism of pharmacological biology in dendrobium plants. *Evid Based Complement Altern Med.* 2015;2015:841752.
- Wang J, Wang L, Kitanaka S. Stilbene and dihydrophenanthrene derivatives from *Pholidota chinensis* and their nitric oxide inhibitory and radical-scavenging activities. *J Nat Med.* 2007;61:381–6.
- Yao S, Tang C-P, Li XQ, Ye Y. Phochinenins A-F, dimeric 9,10-dihydrophenanthrene derivatives, from *Pholidota chinensis*. *Helv Chim Acta.* 2008;91:2122–9.
- Yao S, Tang C-P, Ye Y, Kurtan T, Kiss-Szikszai A, Antus S, et al. Stereochemistry of atropisomeric 9,10-dihydrophenanthrene dimers from *Pholidota chinensis*. *Tetrahedron: Asymmetry.* 2008;19:2007–14.
- Morgan BP. The membrane attack complex as an inflammatory trigger. *Immunobiology.* 2016;221:747–51.
- Reyes-Ramirez A, Leyte-Lugo M, Figueroa M, Serrano-Alba T, Gonzalez-Andrade M, Mata R. Synthesis, biological evaluation, and docking studies of gigantol analogs as calmodulin inhibitors. *Eur J Med Chem.* 2011;46:2699–708.
- Ni X, Gao Y, Wu Z, Ma L, Chen C, Wang L, et al. Functional human induced hepatocytes (hiHeps) with bile acid synthesis and transport capacities: a novel in vitro cholestatic model. *Sci Rep.* 2016;6:38694.
- Wu ZT, Qi XM, Sheng JJ, Ma LL, Ni X, Ren J, et al. Timosaponin A3 induces hepatotoxicity in rats through inducing oxidative stress and down-regulating bile acid transporters. *Acta Pharmacol Sin.* 2014;35:1188–98.
- Gabrielson J, Weiner D. Non-compartmental analysis. *Methods Mol Biol.* 2012;929:377–89.
- Futschik ME, Carlisle B. Noise-robust soft clustering of gene expression time-course data. *J Bioinform Comput Biol.* 2005;3:965–88.
- Yu G, Wang LG, Han Y, He QY. ClusterProfiler: an R package for comparing biological themes among gene clusters. *Omic.* 2012;16:284–7.
- Liu D, Zhao X. Method and application for dynamic comprehensive evaluation with subjective and objective information. *PLoS One.* 2013;8:e83323.
- Podack ER, Tschopp J. Membrane attack by complement. *Mol Immunol.* 1984;21:589–603.
- Qian YM, Qin X, Miwa T, Sun X, Halperin JA, Song WC. Identification and functional characterization of a new gene encoding the mouse terminal complement inhibitor CD59. *J Immunol.* 2000;165:2528–34.
- Pontoglio M, Pausa M, Doyen A, Viollet B, Yaniv M, Tedesco F. Hepatocyte nuclear factor 1alpha controls the expression of terminal complement genes. *J Exp Med.* 2001;194:1683–9.
- Shavva VS, Mogilenko DA, Dizhe EB, Oleinikova GN, Perevozchikov AP, Orlov SV. Hepatic nuclear factor 4alpha positively regulates complement C3 expression and does not interfere with TNFalpha-mediated stimulation of C3 expression in HepG2 cells. *Gene.* 2013;524:187–92.
- Perez MJ, Briz O. Bile-acid-induced cell injury and protection. *World J Gastroenterol.* 2009;15:1677–89.
- Tang D, Kang R, Coyne CB, Zeh HJ, Lotze MT. PAMPs and DAMPs: signal 0s that spur autophagy and immunity. *Immunol Rev.* 2012;249:158–75.
- Jaeschke H. Reactive oxygen and mechanisms of inflammatory liver injury: present concepts. *J Gastroenterol Hepatol.* 2011;26(Suppl 1):173–9.
- Weber LW, Boll M, Stampfl A. Hepatotoxicity and mechanism of action of haloalkanes: carbon tetrachloride as a toxicological model. *Crit Rev Toxicol.* 2003;33:105–36.
- Liu X, Zhang H, Jiang Y. Clinical effect of bicyclol tablet in decreasing plasma ALT/AST levels. *Weichangbingxue He Ganbingxue Zazhi.* 2011;20:751–3.
- Qin X, Gao B. The complement system in liver diseases. *Cell Mol Immunol.* 2006;3:333–40.
- Melgaco JG, Veloso CE, Pacheco-Moreira LF, Vitral CL, Pinto MA. Complement system as a target for therapies to control liver regeneration/damage in acute liver failure induced by viral hepatitis. *J Immunol Res.* 2018;2018:3917032.
- Wang F, Zha WS, Zhang JX, Li SL, Wang H, Ye LP, et al. Complement C3a binding to its receptor as a negative modulator of Th2 response in liver injury in trichloroethylene-sensitized mice. *Toxicol Lett.* 2014;229:229–39.
- Debray FG, de Halleux V, Guidi O, Detrembleur N, Gaillez S, Rausin L, et al. Neonatal liver cirrhosis without iron overload caused by gestational alloimmune liver disease. *Pediatrics.* 2012;129:e1076–9.
- Sun S, Guo Y, Zhao G, Zhou X, Li J, Hu J, et al. Complement and the alternative pathway play an important role in LPS/D-GalN-induced fulminant hepatic failure. *PLoS One.* 2011;6:e26838.
- Marshall KM, He S, Zhong Z, Atkinson C, Tomlinson S. Dissecting the complement pathway in hepatic injury and regeneration with a novel protective strategy. *J Exp Med.* 2014;211:1793–805.
- Bykov I, Junnikkala S, Pekna M, Lindros KO, Meri S. Complement C3 contributes to ethanol-induced liver steatosis in mice. *Ann Med.* 2006;38:280–6.
- Pritchard MT, McMullen MR, Stavitsky AB, Cohen JI, Lin F, Edward Medof M, et al. Differential contributions of C3, C5, and decay-accelerating factor to ethanol-induced fatty liver in mice. *Gastroenterology.* 2007;132:1117–26.
- Rensen SS, Slaats Y, Driessen A, Peutz-Kootstra CJ, Nijhuis J, Steffensen R, et al. Activation of the complement system in human nonalcoholic fatty liver disease. *Hepatology.* 2009;50:1809–17.
- Amara U, Flierl MA, Rittirsch D, Klos A, Chen H, Acker B, et al. Molecular intercommunication between the complement and coagulation systems. *J Immunol.* 2010;185:5628–36.
- Davies A, Lachmann PJ. Membrane defence against complement lysis: the structure and biological properties of CD59. *Immunol Res.* 1993;12:258–75.
- Garnier G, Circolo A, Colten HR. Constitutive expression of murine complement factor B gene is regulated by the interaction of its upstream promoter with hepatocyte nuclear factor 4. *J Biol Chem.* 1996;271:30205–11.
- Zhang J, Hu W, Xing W, You T, Xu J, Qin X, et al. The protective role of CD59 and pathogenic role of complement in hepatic ischemia and reperfusion injury. *Am J Pathol.* 2011;179:2876–84.
- Fondevila C, Shen XD, Tsuchihashi S, Uchida Y, Freitas MC, Ke B, et al. The membrane attack complex (C5b-9) in liver cold ischemia and reperfusion injury. *Liver Transpl.* 2008;14:1133–41.
- Thorgersen EB, Barratt-Due A, Haugaa H, Harboe M, Pischke SE, Nilsson PH, et al. The role of complement in liver injury, regeneration, and transplantation. *Hepatology.* 2019;70:725–36.
- Lee M, Narayanan S, McGeer EG, McGeer PL. Aurin tricarboxylic acid protects against red blood cell hemolysis in patients with paroxysmal nocturnal hemoglobinemia. *PLoS One.* 2014;9:e87316.